

# Study on Acoustic and Flow Induced Noise Characteristics of T-Shaped Pipe with Square Cross-Section

Masaaki Mori<sup>\*1</sup>, Takayuki Masumoto<sup>2</sup>, Kunihiko Ishihara<sup>3</sup>

<sup>1,2</sup> Mechanical CAE Division, CYBERNET SYSTEMS CO.,LTD., 3 Kanda-neribeicho, Chyoda-ku, Tokyo, 101-0022, Japan

<sup>3</sup> Department of Health and Welfare, Tokushima Bunri University, Shido, Sanuki-city, Kagawa, 769-2193, Japan

<sup>\*</sup>1m-mori@cybernet.co.jp; <sup>2</sup>masumoto@cybernet.co.jp; <sup>3</sup>k-ishihara@fe.bunri-u.ac.jp

## Abstract

An aerodynamic sound generated by a flow inside a pipe is one of the noise problems. In addition to the aerodynamic sound sources, characteristics of the generated sound are sometimes affected by acoustic and vibration characteristics of the pipe. In this paper, we have performed experiments and simulations to clarify acoustic and flow induced sound characteristics of a T-shaped pipe with a square cross-section. The experiments and simulations were performed under several inflow velocity conditions. The results show that the characteristics of the flow induced sound in the pipe are strongly affected by the acoustic characteristics of the pipe interior sound field. The frequency characteristics of the sound sources generated by the flow depend on the inflow velocity conditions. However, that of the generated sound does not depend on the inflow velocity conditions, but on the acoustic frequency characteristics of the pipe.

## Keywords

*Flow-induced noise; Lighthill's acoustic analogy; BEM; Acoustic Characteristics; Structure-Acoustic Coupling*

## Introduction

An aerodynamic sound generated by a flow inside a pipe or a duct is one of the noise problems in the equipment such as air conditioner. An air conditioner consists of a duct, fan and openings. There are three types of flow induced sound sources in the air conditioner. One is the sound sources generated by the fan, so-called fan noise. The second is the sound sources generated by the flow around bending or expanding parts of the duct. The third is the sound sources generated by the flow near openings. However, it is still incompletely understood that which type of the sound sources is dominant. In order to reduce the noise, it is necessary to know the dominant sound sources.

Studies on the aerodynamic sound generated inside the duct have been done experimentally. Watanabe et al. investigated the acoustic power level generated by the air flow in duct systems [1]. Itamoto and Shiokawa studied flow noise and sound characteristics of glass fiber ducts [2], [3]. Their research results are also used as data collection. Ishihara investigated acoustic and flow noise characteristics of straight and bending duct with some openings [4], [5], [6]. It is clarified that the noise reduction effect of the absorbing treatment could be neglected when noise sources were generated only by the flow. The noise reduction effects due to bending and use of inner guides or airfoils were clarified. In the case of pipe noise, Hambric et al. studied the flow-induced vibration and acoustic power spectra of a 90° piping elbow and proposed a procedure of the coupling of CFD and structural-acoustic models [7]. Zhang et al. studied the flow-induced vibration and noise of a 90° piping elbow and the effect of guide vanes [8]. They computed the hydrodynamic noise based on a hybrid LES/Lighthill's acoustic analogy [9] and clarified the effective position of guide vanes in reducing vibration and flow-induced noise in the 90° piping elbow with water. However, to the author's knowledge, there have not been many studies focused on effects of both acoustic and vibration characteristics of pipes on aerodynamic sounds.

The purpose in this paper is to clarify the effect of the acoustic and vibration characteristics of the pipe on the aerodynamic sound. We have performed both experiments and simulations of aerodynamic sounds generated by the flow in the T-shaped pipe with the square cross-section. To predict aerodynamic sounds computationally, the hy-

brid CFD/BEM method [10], [11] is applied. The mode shapes are calculated by means of FEM, and the acoustic characteristics are calculated by means of BEM including the structure-acoustic coupling effect.

## Numerical Procedure

### *Transient CFD Simulation*

The transient flow fields in the T-shaped pipe with the square cross-section of a length  $D = 100\text{mm}$  on a side are simulated at Reynolds numbers,  $\text{Re} = 41075$  and  $78728$ . Inflow velocities are  $U = 6$  and  $11.5\text{m/s}$ . Mach numbers are  $M=0.0177$  and  $M=0.0338$ , respectively. Figure 1 shows a computational domain and schematic diagram. For these simulations, the three-dimensional computational domain in the T-shaped pipe has been applied, as shown in Fig.1. Unsteady flow fields are calculated using the commercial CFD code ANSYS Fluent version 15.0 and its incompressible LES (Dynamic Smagorinsky model) calculation features. The origin of the Cartesian coordinate is placed at the midpoint of the pipe. The domain contains 544,000 hex cells and 573,221 nodes. The cell spacing adjacent to the wall is  $0.8\text{mm}$  ( $0.008D$ ). Steady velocities are imposed on the inflow boundary. Pressure boundary conditions are applied on the outflow boundaries. No-slip conditions are applied on the other walls. Steady state simulations were performed using Spalart-Allmaras (S-A) turbulence model and then used as initial conditions of transient LES simulations. The transient simulations were performed for 7,800 time steps with a time step size  $\Delta t = 1\text{e-4s}$ , which corresponds to a Courant-Fredrichs-Lowy (CFL) number of 2.1.

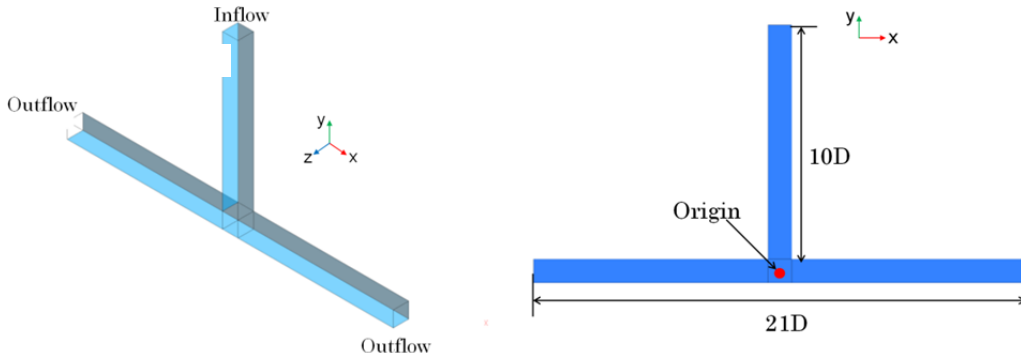


FIG. 1 DOMAIN SHAPE AND SCHEMATIC DIAGRAM

### *Lighthill Equation*

Lighthill equation [12], [13] in the frequency domain is derived from the equation of continuity and compressible Navier-Stokes equation and as follows:

$$(\nabla^2 + k^2)p = -\frac{\partial^2 T_{lm}}{\partial x_l \partial x_m}, \quad (1)$$

where  $p$  is the acoustic pressure,  $k$  is the wave number,  $c$  is the speed of sound,  $l$  and  $m$  indicate each direction in the Cartesian coordinates,  $v$  is the flow velocity.  $T_{lm}$  is the Lighthill stress tensor and as follows:

$$T_{lm} = \rho v_l v_m + (p - c^2 \rho) \delta_{lm} - \tau_{lm}, \quad (2)$$

where  $\rho$  is the density and  $1.225\text{kg/m}^3$ ,  $\delta_{ij}$  is the Kronecker delta and  $\tau_{lm}$  is the viscous stress tensor. For a low Mach number and high Reynolds number flow regime, the second and third terms of equation (2) are negligible [8], [10], [14]. Therefore, the first term is used for the present work.

### *Extraction of Acoustic Source*

To convert the acoustic source time histories into the frequency spectra, the discrete Fourier transform (DFT) has been applied. The acoustics sources are extracted from 512 steps (from  $t = 0.52\text{s}$  to  $0.6222\text{s}$ ) flow field data, the sampling period is  $2\text{e-4s}$ .

### *Acoustic Calculation*

The acoustic characteristics are solved using the commercial BEM code WAON. In this solver, the following simul-

taneous linear equation is solved:

$$(\mathbf{E} + \mathbf{B} + \mathbf{C})\mathbf{p} = j\omega\rho\mathbf{Av} + \mathbf{p}_d, \quad (3)$$

Here,  $\mathbf{p}$  is the acoustic pressure vector,  $\mathbf{v}$  is the particle velocity vector and the entries of the influence coefficient matrices are represented as follows:

$$E_{ij} = \frac{1}{2}\delta_{ij}, \quad (4)$$

$$A_{ij} = \int_{\Gamma_V} N_j(\mathbf{r}_q)G(\mathbf{r}_i, \mathbf{r}_q)dS_q, \quad (5)$$

$$B_{ij} = \int_{\Gamma_A} N_j(\mathbf{r}_q) \frac{\partial G(\mathbf{r}_i, \mathbf{r}_q)}{\partial n_q} dS_q, \quad (6)$$

$$C_{ij} = \frac{jk}{Z_j} \int_{\Gamma_A} N_j(\mathbf{r}_q)G(\mathbf{r}_i, \mathbf{r}_q)dS_q, \quad (7)$$

where  $\delta_{ij}$  is Kronecker delta, and  $\Gamma$  is the total boundary.  $\Gamma_V$  is a part of  $\Gamma$  where the surface is assumed to be vibrating.  $\Gamma_A$  is also a part of  $\Gamma$  where the surface absorbs acoustic wave.  $\mathbf{r}_i$  is a position vector of the  $i$ -th node,  $\mathbf{r}_q$  is a position vector of the source point q, and  $N_j$  is the interpolation function of the  $j$ -th node.

With the number of nodes  $N$ , the component  $p$  of the vector  $\mathbf{p}$  is as follows:

$$p(\mathbf{r}_q) = \sum_{j=1}^N N_j(\mathbf{r}_q)p_j. \quad (8)$$

The component  $p_d$  of the vector  $\mathbf{p}_d$  is the direct pressure contribution from the acoustic source, which is evaluated by the following equation:

$$p_d(\mathbf{r}_p) = \frac{1}{4\pi} \frac{\partial^2}{\partial x_l \partial x_m} \int_{-\infty}^{\infty} \frac{T_{lm}(\mathbf{r}_s, \omega) e^{jk|\mathbf{r}_p - \mathbf{r}_s|}}{|\mathbf{r}_p - \mathbf{r}_s|} dV \quad (9)$$

where  $\partial^2/\partial x_l \partial x_m$  is the directional derivative and V is the volume of the flow field (in this case, the region filled by CFD cell).  $\mathbf{r}_p$  is a position vector of the monitor point p, and  $\mathbf{r}_s$  is a position vector of the source point s.

There are 2,780 boundary elements. The acoustic sources are extracted from CFD results, whose numbers are equivalent to the number of grids of the CFD model. Figure 2 shows the boundary elements. To concern acoustic waves moving from the inflow boundary to the outside, an impedance boundary condition is imposed at the inflow boundary. The value of the impedance is  $\rho c$ . In the structure-acoustic coupled model, all surfaces other than inflow boundary are boundaries where the structure-acoustic coupling effect is considered. In the uncoupled model, they are assumed to be rigid.

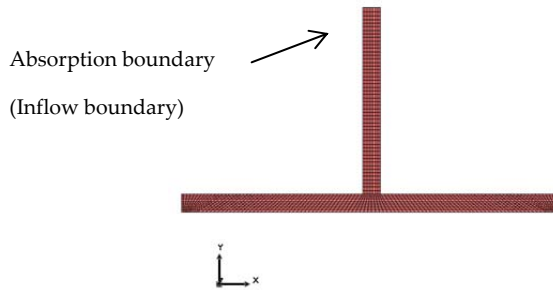


FIG. 2 BOUNDARY ELEMENT MESH

### Structural-Acoustic Coupling

In this paper, the structural-acoustic coupled model is solved. In order to solve structural-acoustic coupled model, equations corresponding to the acoustic field and structure must be solved simultaneously.

Displacement of the structure is described using equation of motion as follows:

$$(-\omega^2 \mathbf{M} + j\omega \mathbf{C} + \mathbf{K})\mathbf{u} = \mathbf{f}_s, \quad (10)$$

where  $\mathbf{M}$  is the Mass matrix,  $\mathbf{C}$  is the Damping matrix,  $\mathbf{K}$  is the Stiffness matrix and  $\mathbf{f}_s$  is the excitation force vector.

With modal coordinates, Equation (10) is expressed as follows:

$$(-\omega^2 + 2jh\omega\omega_0 + \omega_0^2)\mathbf{q} = \boldsymbol{\varphi}^T \mathbf{f}_s, \quad (11)$$

where  $h$  is the modal damping ratio,  $\omega_0$  is the matrix in which eigenvalues are arranged diagonally,  $\boldsymbol{\varphi}^T$  the eigenvector transposition, and  $\mathbf{q}$  the modal participation factor.

In order to consider the acoustic contribution to the structural model, an additional force term from the acoustic field is introduced as follows:

$$(-\omega^2 + 2jh\omega\omega_0 + \omega_0^2)\mathbf{q} = \boldsymbol{\varphi}^T (\mathbf{f}_s - \mathbf{p}_s), \quad (12)$$

where  $s$  is the area affected by the acoustic pressure.

On the other hand, to consider the structural contribution to the acoustic model, an additional velocity term from the structure is introduced to Equation (3):

$$(\mathbf{E} + \mathbf{B} + \mathbf{C})\mathbf{p} = j\omega\rho\mathbf{A}\mathbf{v} + j\omega\rho\mathbf{A}'\mathbf{v}_s + \mathbf{p}_d, \quad (13)$$

here  $\mathbf{v}_s$  the vibration velocity vector of the structural model and,

$$\dot{A}_{ij} = \int_{\Gamma_3} N_j(\mathbf{r}_q) G(\mathbf{r}_i, \mathbf{r}_q) dS_q, \quad (14)$$

where  $\Gamma_3$  is the boundary on which structural-acoustic coupling effect is considered.  $\Gamma_3$  corresponds to all of the surfaces other than the inflow boundary in Fig.2.

The term  $\mathbf{v}_s$  in Equation (13) is modified into an expression in which modal coordinates are used. Combining Equation (12) and (13), we obtain the following coupled equation of acoustic and structural models:

$$\begin{bmatrix} \mathbf{E} + \mathbf{B} + \mathbf{C} & \omega^2\rho\mathbf{A}'\boldsymbol{\varphi} \\ -\boldsymbol{\varphi}^T s & -\omega^2 + 2jh\omega\omega_0 + \omega_0^2 \end{bmatrix} \begin{Bmatrix} \mathbf{p} \\ \mathbf{q} \end{Bmatrix} = \begin{Bmatrix} j\omega\rho\mathbf{A}\mathbf{v} + \mathbf{p}_d \\ \boldsymbol{\varphi}^T \mathbf{f}_s \end{Bmatrix}. \quad (15)$$

The modal information of the pipe has been extracted using ANSYS Mechanical version 15.0. Figure 3 shows boundary conditions in the modal analysis.

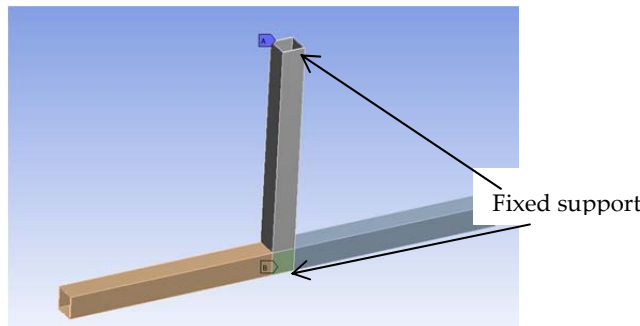
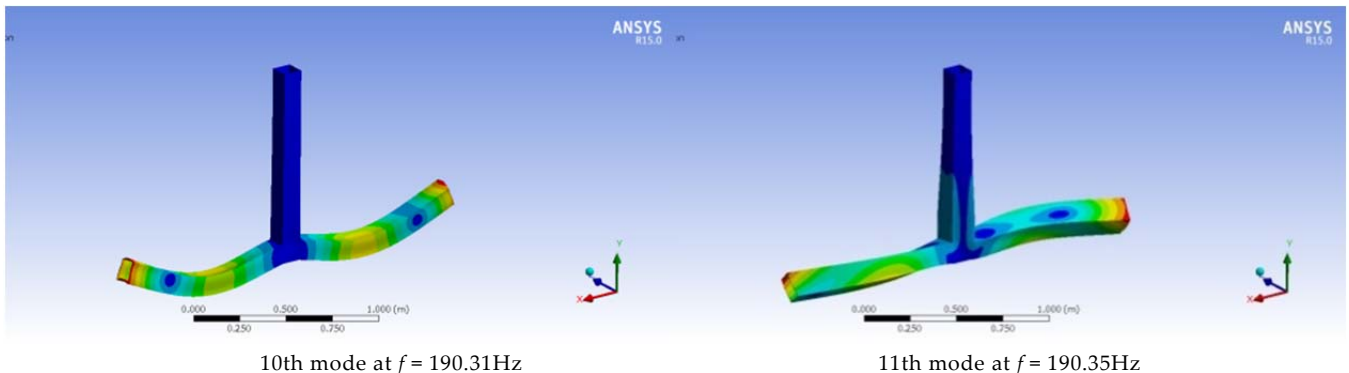


FIG. 3 BOUNDARY CONDITIONS IN THE MODAL ANALYSIS

Young's Modulus, Poisson's ratio and density of the T-rectangular pipe are respectively, 3.14GPa, 0.35 and 1190kg/m<sup>3</sup>. The damping ratio is 0.05 (5%). The thickness of the pipe is 5mm. As the result of the modal analysis, typical mode shapes are obtained, as shown in Fig. 4.



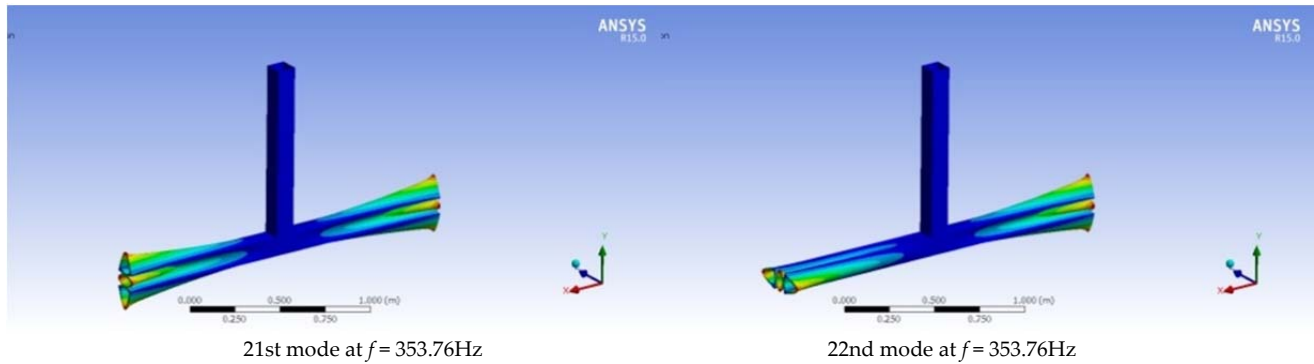


FIG. 4 TYPICAL SHAPE MODES OF MODAL ANALYSIS

## Experimental Setup

Experimental setup is shown in Fig. 5. With a microphone that is placed at 100mm from the centre of the outflow boundary, sound pressure signals are measured and converted to frequency domain with FFT Analyser. The frequency range is from 20Hz to 1000Hz, the sampling frequency is 10000Hz, the number of averages is 1000, and the frequency resolution is 10Hz. Inflow velocities are about 6, 8, 10, 11.5m/s. Background sound pressure level is below 30dB.

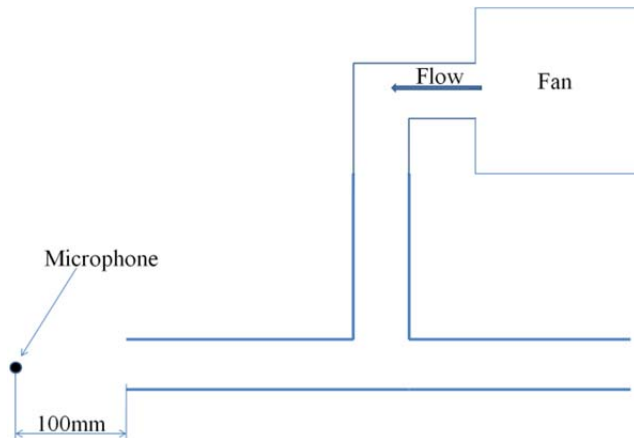
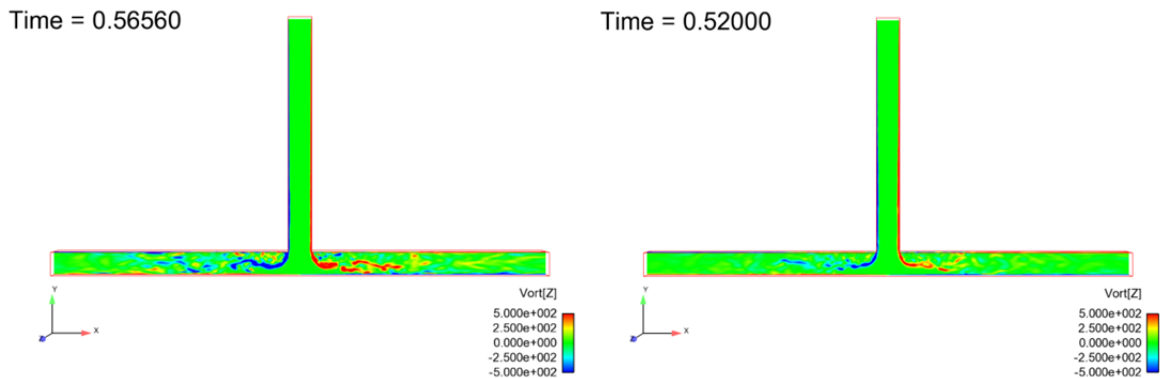
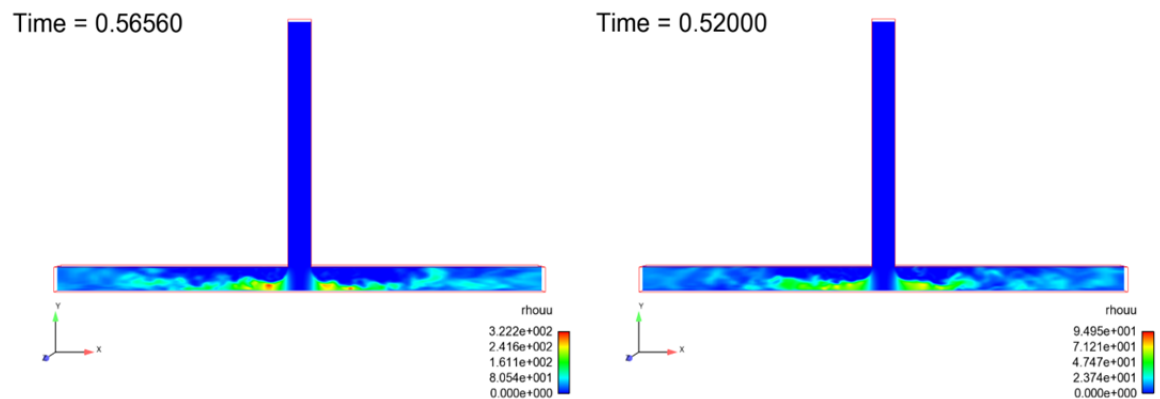
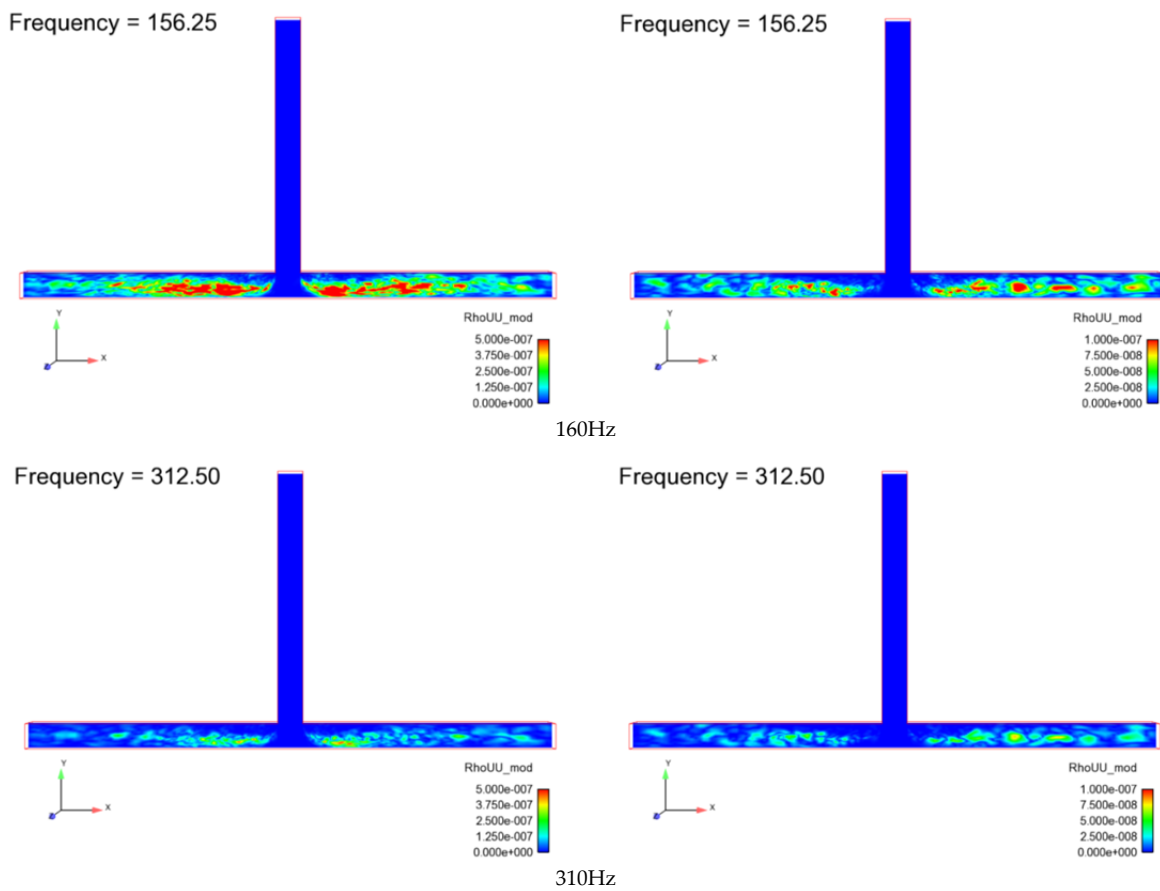


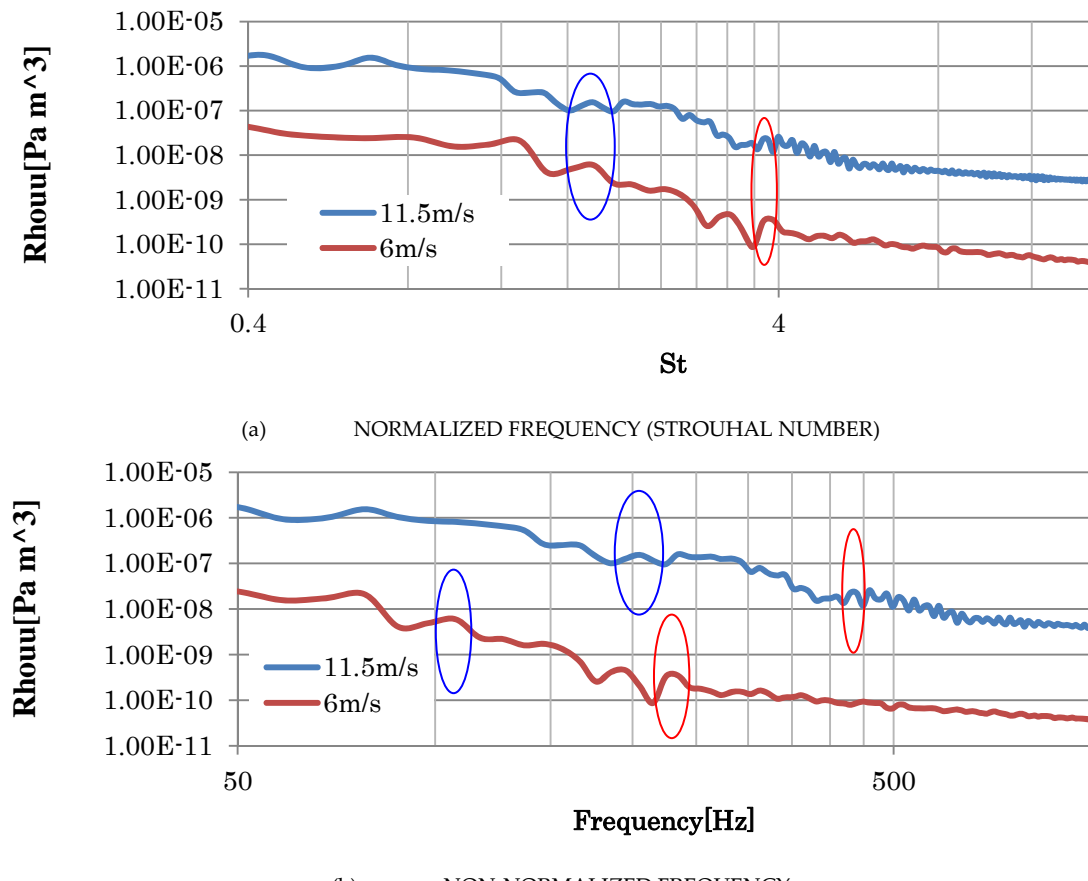
FIG. 5 EXPERIMENTAL SETUP

## Results and Discussion

### Transient CFD Results

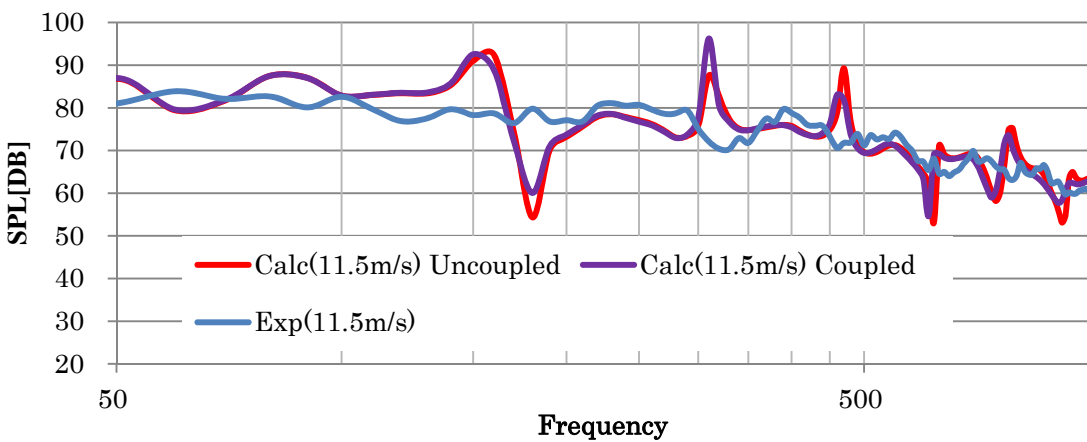
Instantaneous snapshots of the vorticity field at  $Z = 0$  plane are shown in Fig. 6. Vortices generated near corners of the pipe are shed from the corner and travels downstream. Shed vortices merge and interact with the pipe wall. Motions of these vortices play an important role of the sound generation. Figure 7 shows instantaneous snapshots of the Lighthill stress tensor  $\rho v_l v_m$  at  $Z = 0$  plane. Significant acoustic sources exist near corners and the wall of the pipe in Fig. 7, as in the vorticity field. Figure 8 shows the magnitude of the volumetric acoustic sources (Lighthill stress tensor) extracted from the CFD results. As shown in Fig. 8, magnitudes of the acoustic sources are relatively symmetry with respect to the YZ plane. The frequency spectra of the volumetric Lighthill stress tensor  $\rho v_1 v_1$  at  $(1D, 0, 0)$  are shown in Fig. 9. Figure 9 (a) shows the spectra of normalized frequency (Strouhal number,  $St = fD/U$ ), and Figure 9 (b) shows the spectra of non-normalized frequency. Some outstanding peaks are surrounded by blue and red circles, as shown in Fig. 9 (a) and (b). The Strouhal numbers of the peak surrounded by the blue and red circles are  $St=1.78$  and  $3.74$ , respectively in Fig. 9 (a). The Strouhal number,  $St=1.78$  corresponds with  $205.1[\text{Hz}]$  at  $U=11.5\text{m/s}$  and  $107[\text{Hz}]$  at  $U=6\text{m/s}$  in Fig. 9 (b), respectively. In the same way, the Strouhal number,  $St=3.74$  corresponds with  $429.9[\text{Hz}]$  at  $U=11.5\text{m/s}$  and  $224.3[\text{Hz}]$  at  $U=6\text{m/s}$ , respectively in Fig. 9 (b). Therefore, it is clear that the peak frequencies of the acoustic sources depend on the inflow velocity.

FIG. 6 INSTANTANEOUS SNAPSHOTS OF VORTICITY FIELD AT  $Z=0$  PLANE (LEFT: 11.5 m/s, RIGHT: 6 m/s)FIG. 7 INSTANTANEOUS SNAPSHOTS OF LIGHTHILL STRESS TENSOR  $\rho v_l v_m$  AT  $Z=0$  PLANE (LEFT: 11.5 m/s, RIGHT: 6 m/s)FIG. 8 MAGNITUDE OF VOLUMETRIC ACOUSTIC SOURCES  $\rho v_l v_m$  AT  $Z=0$  PLANE (LEFT: 11.5 m/s, RIGHT: 6 m/s)

FIG. 9 SPECTRUM OF LIGHTHILL STRESS TENSOR  $\rho v_1 v_1$  PER UNIT VOLUME

### *Far-Field Acoustics*

To investigate the effect of the structural-acoustic coupling on the far-field sound pressure, we have calculated sound pressure fields in both cases of the coupled and uncoupled model using the acoustic sources extracted from the CFD results. Figure 10 shows the comparison of sound pressure levels in the cases of the coupled and uncoupled model. The position of the monitor point is shown in Fig.5. Peak levels of the sound pressure in the case of the coupled model are smaller than those in the case of the uncoupled model. However, there is no significant difference between the coupled and uncoupled model in terms of the frequency characteristics of the far-field sound pressure. It indicated that there is relatively small effect of the structure vibration on the far-field sound pressure in the present work.

FIG. 10 COMPARISON OF SOUND PRESSURE LEVELS IN THE CASES OF THE COUPLED AND UNCOUPLED AT  $U = 11.5\text{m/s}$ .

Figures 11 and 12 show the frequency spectra of SPL at the position. Both the simulated and measured data are shown in Fig. 11, and only the measured data are shown in Fig. 12. Comparing the simulated and measured spectra, the simulated spectra have some intense peaks. It is likely that the difference between the measured and simulated is attributed to the acoustic damping. Therefore, we have calculated the structural – acoustic coupled responses with the weak sound absorption on all boundaries except the inlet. The absorption coefficient is 0.05 in the present work. Figure 13 shows the frequency spectra of SPL with the weak sound absorption. The intense peaks are suppressed. There is a possibility that an acoustic damping in addition to the structural damping acts in the experiment. In regard to the acoustic damping, it is necessary to consider for our future work.

As shown in Fig.9, the frequency characteristics of the acoustic sources depend on the inflow velocity. However, both the measured and simulated frequency characteristics of SPL do not depend on the inflow velocity, and peak frequencies of SPL are almost the same between 11.5 m/s and 6 m/s cases, as shown in Figs. 11, 12 and 13. Figure 14 shows contours of the sound pressure field. Depending on the inflow velocity, magnitudes of the sound pressure are different between the two cases. However, directivities of the sound pressure do not depend on the inflow velocity, and they are almost the same in the two cases. Table 1 shows the overall sound pressure level (OASPL) (50-1000Hz). The OASPLs of the measured and simulated data show a relatively good agreement.

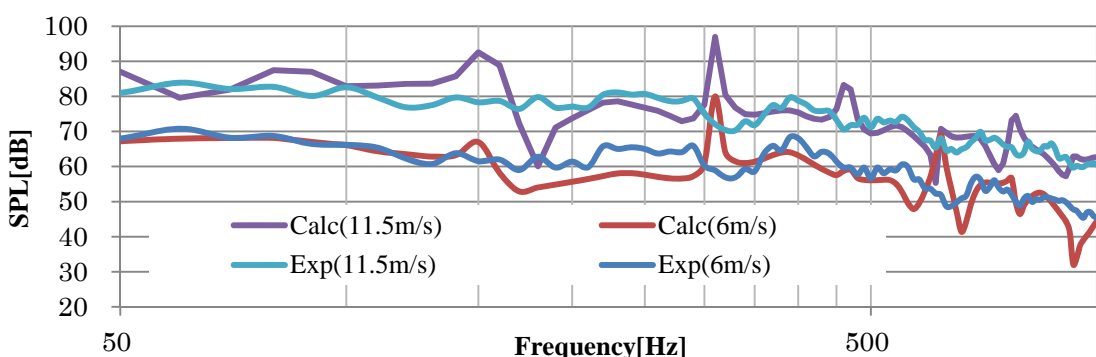


FIG. 11 SPECTRUM OF SPL NEAR THE OUTFLOW BOUNDARY

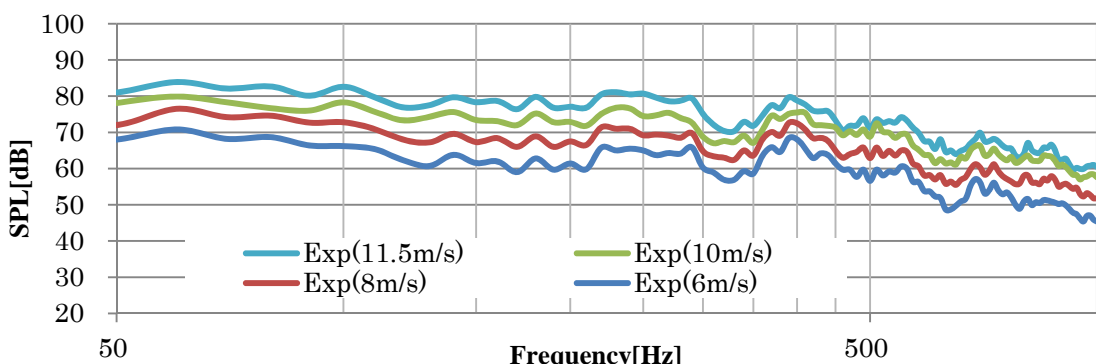


FIG. 12 SPECTRUM OF SPL NEAR THE OUTFLOW BOUNDARY (MEASURED)

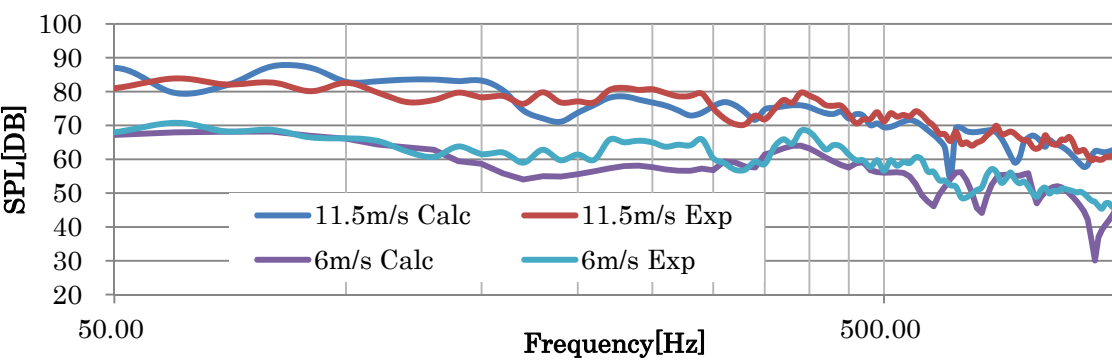


FIG. 13 SPECTRUM OF SPL NEAR THE OUTFLOW BOUNDARY WITH WEAK ACOUSTIC ABSORPTION

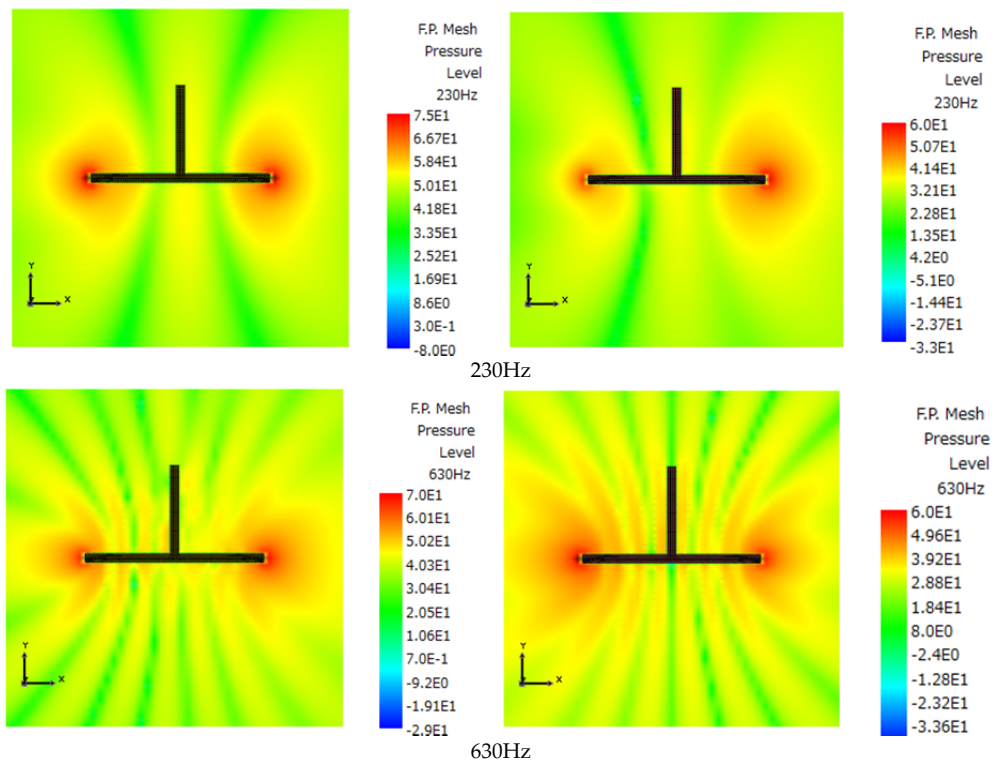
FIG. 14 SOUND PRESSURE FIELD AT  $Z=0$  PLANE (LEFT:  $U = 11.5\text{m/s}$ , RIGHT:  $U=6\text{m/s}$ )

TABLE 1 OVERALL SOUND PRESSURE LEVEL (50HZ-1000HZ)

Inflow Velocity	Measured	Simulated	Simulated (Weak Absorption)
6m/s	90.1dB	91.8dB	89.22dB
8m/s	95.3dB	---	---
10m/s	100.2dB	---	---
11.5m/s	104.3dB	109.8dB	104.96dB

### Acoustic Characteristic of the Pipe

As shown in Fig.12, peak frequencies of SPL do not depend on the inflow velocity. Therefore, it can be presumed that the acoustic modes of the pipe interior sound field strongly affect the frequency characteristics of the flow induced sound in the pipe. To clarify the acoustic characteristic of the pipe, the acoustic frequency responses have been calculated using the monopole point sources (without the flow) shown in Fig.15. To examine the position dependence of the sound source, two types of analysis models are used, as shown in Fig.15. In the case of Type 1, the point source is located at the origin ("Symmetric source" position case). In the case of Type 2, the point source is located at  $(4D, 0, 0)$  ("Asymmetric source" position case). The magnitude of the point sources is 1Pa in all frequencies. Figure 16 shows acoustic frequency characteristics of the pipe (without the flow). The measured data (with the flow) is also plotted in Fig.16. Some outstanding peaks are surrounded by red and blue circles in Fig.16. Some acoustic modes of the pipe are also shown in Fig. 17. Figure 16 and Figure 17 show that in the case of Type 2, more acoustic modes are excited than in the case of Type 1. Comparing the cases of Type 1 and Type 2, in the case of Type 1, the simulated data is smooth and similar to the measured data (with the flow). However, in the case of Type 2, some acoustic modes (peaks surrounded by the red circle) appear and their modes also appear in the measured data. The results show that the acoustic frequency characteristics of the pipe depend on the position of the acoustic source, and are similar to the frequency characteristics of the flow induced sound in the pipe in terms of the peak frequency. Also, the results explain that the frequency characteristics of the flow induced sound in the pipe are affected by the acoustic frequency characteristics of the pipe.

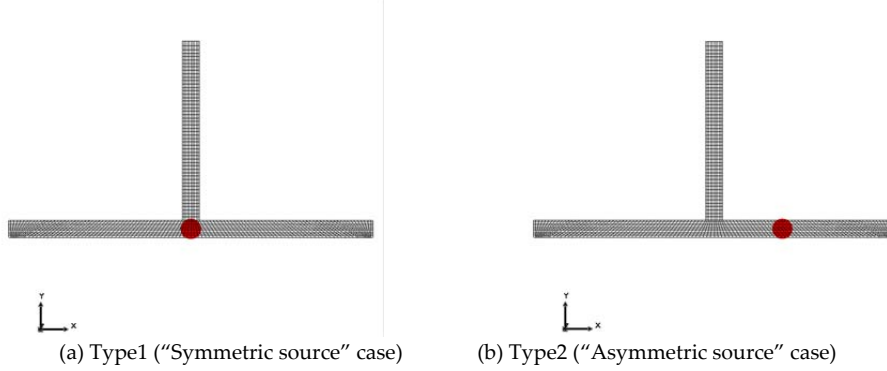


FIG. 15 ACOUSTIC SOURCES FOR THE FREQUENCY RESPONSE ANALYSIS

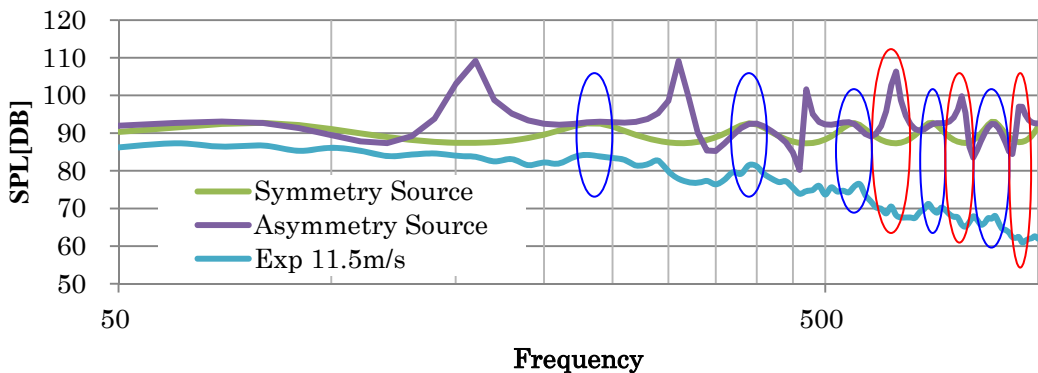


FIG. 16 ACOUSTIC FREQUENCY CHARACTERISTIC OF THE PIPE (WITHOUT THE FLOW)

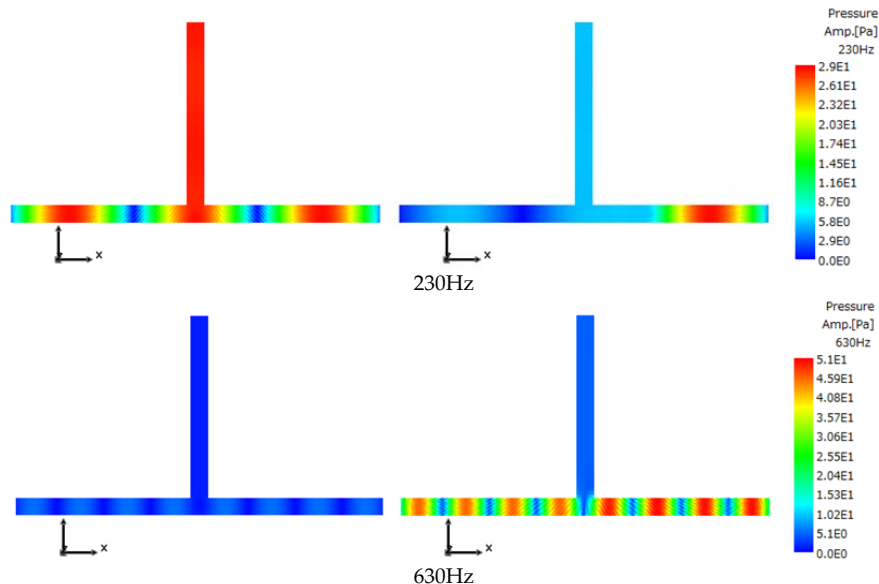


FIG. 17 ACOUSTIC MODE OF THE PIPE (LEFT: TYPE1 (SYMMETRIC SOURCE), RIGHT: TYPE2 (ASYMMETRIC SOURCE))

## Conclusions

In this paper, we have performed the experiments and simulations on the acoustic, vibration and aerodynamic sound characteristics of the T-shaped rectangular cross-sectional pipe. The experiments and simulations were performed under several inflow velocity conditions. The following concluding remarks are obtained in this paper.

- (1) To investigate the effect of the structural-acoustic coupling on the far-field sound pressure, the structure-acoustic coupled and uncoupled model are calculated using the acoustic sources extracted from the CFD results. The effect of the structure vibration on the far-field sound pressure is relatively small in the present work.

- (2) Magnitudes of the generated aerodynamic sound pressure vary depending on the inflow velocity. However, the directivities and frequency characteristics of the sound pressure do not depend on the inflow velocity, and they are almost the same for all inflow velocities.
- (3) The acoustic frequency responses of the pipe interior sound field were calculated using two types of the monopole point sources (without the flow). The acoustic frequency characteristics of the pipe depend on the position of the acoustic source. In terms of the peak frequency, they are similar to the frequency characteristics of the flow induced sound in the pipe. The results explain that the frequency characteristics of the aerodynamic sound in the pipe are affected by the acoustic frequency characteristic of the pipe.

The further study of the case that the thickness of the pipe is reduced is underway to clarify the effect of the structural-vibration on the far-field sound.

#### REFERENCES

- [1] Watanabe, Kaname et al. "A Study on Noise Generated by the Air Flow in Duct System." *Journal of the Society of Heating, Air-Conditioning and Sanitary Engineers of Japan* 37 (5) (1963): 22-33.
- [2] Shiokawa, Hiroshi, and Itamoto, Morimasa. "On Sound Characteristics of Straight Glass Fiber Ducts." *Journal of Architecture, Planning and Environmental Engineering, Architectural Institute of Japan* 435 (1993): 9-15.
- [3] Itamoto, Morimasa, and Shiokawa, Hiroshi. "On Generated Noise by Air Flow at Straight Glass Fiber Ducts." *Journal of Architecture, Planning and Environmental Engineering, Architectural Institute of Japan* 428 (1991): 21-27.
- [4] Ishihara, Kunihiko. "Study on Acoustics Characteristics of Straight Duct with Some Holes." *Transactions of the Japan Society of Mechanical Engineers* 74 (2008):332-338.
- [5] Ishihara, Kunihiko. "Flow Noise Characteristics Generated from Straight Duct with Some Holes." *Transactions of the Japan Society of Mechanical Engineers* 74 (2009):2521-2528.
- [6] Ishihara, Kunihiko. "Study on Acoustics and Flow Noise Characteristics of Bending Duct." *Transactions of the Japan Society of Mechanical Engineers* 77(2011):1282-1291.
- [7] Hambric, S. A., Boger, D. A., Fahline, J. B. and Campbell, R. L. "Structure- and fluid-borne acoustic power sources induced by turbulent flow in 90° piping elbows." *Journal of Fluids and Structures* 26 (2010):121-147.
- [8] Zhang, T., Zhang, Y., and Ouyang, H. "Structural vibration and fluid-borne noise induced by turbulent flow through a 90 piping elbow with/without a guide vane" *International Journal of Pressure Vessels and Piping* 125 (2015):66-77.
- [9] Zhang, Y., Zhang, T., Ouyang, H., and Li, T. Y., "Flow-induced noise analysis for 3D trash rack based on LES/Lighthill hybrid method" *Applied Acoustics* 77 (2014):141-152.
- [10] Croaker, Paul, Kessissoglou, Nicole, and Marburg, Steffen. "A CFD-BEM coupling technique for low Mach number flow induced noise" *Proceedings of Acoustics 2013*, Victor Harbor, (2013).
- [11] Mori, Masaaki, Masumoto, Takayuki and Ishihara, Kunihiko., Oshima, Takuya., Yasuda, Yosuke., and Sakuma, Tetsuya. "Study on modelling of flow induced noise using Lighthill's analogy and boundary element method." *Proceedings of Internoise2014*, Melbourne, (2014).
- [12] Lighthill, Michael James. "On sound generated aerodynamically, I. General theory." *Proceedings of the Royal Society of London Series A* 211 (1952):564-587.
- [13] Lighthill, Michael James. "On sound generated aerodynamically, II. Turbulence as source of sound" *Proceedings of the Royal Society of London Series A* 222 (1954):1-32.
- [14] Howe, Michael, S. *Theory of Vortex Sound*: Cambridge University Press, 2003.

**Masaaki Mori** graduated Tohoku University in 2001. He received a Master's degree in Aerospace Engineering from Tohoku University in 2003; a Ph.D. from Tohoku University in 2006. He has been working at Acoustic Analysis Solution Group of Mechanical CAE Division in Cybernet Systems since 2006. He is a Sales and Support Engineer of Acoustic, Fluid Dynamics and Structure Analysis Software. Currently, he has been studying Flow-Induced noise and Vibration.

**Takayuki Masumoto** graduated Aoyama Gakuin University in 1995. He has been working at Acoustic Analysis Solution Group of Mechanical CAE Division in Cybernet Systems since 1995. He has been developing the acoustic analysis software for industrial application. Currently, he has been studying Flow-Induced noise and Vibration.

**Kunihiko Ishihara** graduated Kobe University in 1969 and Graduate school of Kobe University in 1971. He received a Ph.D. in Mechanical Engineering from Osaka University in 1985. He worked in Kawasaki Heavy Industry for 33 years and research vibration and noise problems of many products. He has published many articles more than 80. Almost of these articles were listed in Journal of JSME. (Japan Society of Mechanical Engineer). Professor Ishihara is a member of JSME and ASME, and he took many awards. Currently, he has been studying Mechanical Vibration and Noise Control, Especially Flow-Induced Vibration and Noise.